

Baryonic Feedback across Halo Mass: Impact on the Matter Power Spectrum

Kyle Miller,^{a,1} Surhud More,^b Bhuvnesh Jain^a

^aDepartment of Physics and Astronomy, University of Pennsylvania, Philadelphia, PA 19104, USA

^bInter-University Centre for Astronomy and Astrophysics, Pune, Maharashtra 411007, India

E-mail: mky@sas.upenn.edu, surhud@iucaa.in, bjain@physics.upenn.edu,

Abstract.

Upcoming weak-lensing surveys will probe the matter distribution at a few percent level on nonlinear scales ($k > 1 \text{ h Mpc}^{-1}$) where baryonic feedback from galaxy formation modifies the clustering of matter. Using the IllustrisTNG hydrodynamical simulations, we quantify the mass and radial dependence of baryonic suppression of the matter power spectrum by selectively replacing halos in the collisionless run with their full-physics counterparts. We find that group-scale halos with $\log M_{200\text{m}}/h^{-1}M_\odot \in [13, 14]$ dominate the suppression, contributing a large fraction of the total reduction in power at $k \sim 5 - 30 \text{ h Mpc}^{-1}$. The suppression is smaller on either sides of this mass bin. Correctly reproducing the full suppression of the power spectrum requires accounting for matter redistribution (while enforcing mass conservation) beyond the virial radius of each halo. Crucially, the same group-scale regime produces the strongest and most detectable deviations in group–galaxy lensing, making stacked group lensing a powerful observational test of feedback models. Our results motivate emulators that jointly predict the matter power spectrum and halo–matter correlations including baryonic effects, enabling unbiased cosmological inference from small scales.

Keywords: cosmological simulations, large-scale structure, baryonic effects, dark matter, weak gravitational lensing

¹Corresponding author

Contents

1	Introduction	1
2	Data	3
2.1	Cosmological Simulations	3
3	Methodology	3
3.1	Isolating baryonic effects by halo mass	3
3.2	Measurements of the matter power spectrum	5
4	Results	5
4.1	Halo mass and radial dependence of the baryonic feedback	5
4.2	Impact on the group-galaxy weak lensing signal	9
5	Summary and Discussion	11
5.1	Connections to weak lensing and SZ measurements	12
5.2	Improving Theoretical Models	13
A	Mass Conservation	14

1 Introduction

Weak gravitational lensing is a powerful probe of cosmic structure formation. It enables a direct measurement of the matter distribution in the Universe, without relying on biased tracers such as galaxies or gas. While gravity primarily governs the large-scale evolution of matter, small-scale astrophysical processes can significantly affect this distribution, especially given the statistical precision of ongoing and upcoming weak lensing surveys. In particular, baryonic feedback processes associated with galaxy formation and evolution can modify the matter distribution on small scales.

Mechanisms such as gas ejection by supernovae and active galactic nuclei (AGN) are key drivers of these baryonic effects [1–3]. Gas cooling and galaxy formation tend to pull baryons deeper into halos, thereby enhancing the small-scale power in the matter power spectrum. Conversely, feedback from star formation or AGN can expel baryons from galactic centers, reducing small-scale power and boosting it on larger scales. These opposing mechanisms compete: cooling, star formation and associate feedback typically dominate in low-mass halos, whereas AGN feedback is expected to prevail in more massive systems [2, 4–6].

Accurate cosmological inference from weak lensing observables therefore requires careful marginalization over baryonic effects. However, this task remains difficult due to the complex and poorly understood nature of baryonic physics. Marginalizing without informative priors from complementary observables can substantially degrade the statistical power of small-scale measurements [7, 8]. Moreover, much of the weak lensing signal-to-noise arises from nonlinear scales where baryonic processes are most influential, complicating interpretation. Implementing conservative scale cuts to avoid such nonlinear regimes limits the constraining power of next-generation surveys, and as survey precision improves, the required scale cuts would need to increase further unless baryonic effects are modeled.

Consequently, developing robust models for baryonic effects on small scales is essential. Numerous studies have attempted to quantify these effects using hydrodynamical simulations (e.g. [1, 5, 9, 10]). Yet, modeling baryonic feedback remains challenging due to the wide dynamical range of relevant astrophysical processes. Running cosmologically representative simulations at sufficiently high resolution is computationally demanding, and most simulations rely on subgrid prescriptions to model unresolved physics. Differences in these prescriptions can lead to significant variations in predicted outcomes, underscoring the need for continued refinement and cross-validation of baryonic feedback models.

Improved halo models have been developed to mitigate the impact of baryonic feedback on cosmological inference. These models redistribute matter within halos, either in total or by decomposing it into stellar, gaseous, and dark matter components, using density profiles motivated by hydrodynamical simulations [9–14]. Such models typically include several free parameters that must be calibrated against simulations or marginalized over in cosmological analyses. While this approach can reduce biases in inferred cosmological parameters, it introduces a statistical penalty and potential model dependence if priors from simulations are imposed. Some of these parameters, particularly those related to gas physics, can in principle be constrained using observational data, for example, through the various correlations of the thermal and kinetic Sunyaev–Zel’dovich (SZ) effects. However, these constraints are often degenerate with cosmological parameters [6, 14, 15].

Recent efforts to constrain baryonic effects directly from observations such as tSZ and kSZ cross-correlations and weak lensing, have primarily focused on feedback signatures in group- and cluster-scale halos ($M_{200m} > 10^{13} M_{\odot}$) (e.g. [7, 16–22]). However, there has been little direct investigation into which halo mass or spatial scales most strongly influence baryonic effects observable in the cosmic shear signal. Current cosmic shear measurements extending to small scales have shown conflicting claims about the evidence for baryonic feedback effects. For example, [23] show that cosmological inference is unaffected even after including information from small scales and using collisionless predictions to fit the data. This could presumably be due to degeneracies in the baryonic feedback and other systematic effects. However, [24] carry out a joint analysis of galaxy and CMB lensing and suggest the presence of some suppression of the power spectrum on small scales. On the other hand, [22] claim a large suppression in the matter power spectrum due to baryonic feedback effects in a joint analysis of X-ray, kinetic SZ and weak lensing analysis of groups and galaxy clusters. This motivates the development of new observables and joint inference frameworks capable of breaking degeneracies in a data-driven manner, enabling simultaneous inference of cosmological parameters and baryonic feedback effects.

In this work, we use the ILLUSTRIS TNG-300 simulation suite to quantify the contribution of halos in different mass bins to the suppression of the matter power spectrum. By matching halos between the collisionless and full-physics simulations, we construct hybrid snapshots in which selected gravity-only halos are replaced by their baryonic counterparts. We then measure the resulting suppression of the matter power spectrum and examine how this suppression manifests in the group–galaxy lensing signal. This approach allows us to isolate the impact of baryonic feedback across both halo mass and spatial scales. Finally, we discuss how combining cosmic shear and group–galaxy lensing, especially when binned by group properties, can help disentangle baryonic effects from cosmological parameters.

Throughout this work, we will assume that halo masses are defined as M_{200m} , i.e., within a spherical boundary that encompasses 200 times the mean matter density of the Universe. We will use comoving coordinates to describe the scales involved.

2 Data

2.1 Cosmological Simulations

The IllustrisTNG simulation [25–29] is a suite of gravo-magnetohydrodynamic simulations, built with an improved treatment of baryonic physics from the original Illustris simulation suite [30–33] using the moving-mesh AREPO code [34, 35]. A flat Λ CDM cosmology is used with the parameter values $\Omega_m = 0.3089$, $\Omega_b = 0.0486$, $\sigma_8 = 0.8159$, $n_s = 0.9667$ and $H_0 = 67.74 \text{ km s}^{-1} \text{Mpc}^{-1}$.

We focus on the TNG300-1 (full-physics) and TNG300-1-Dark (gravity-only) runs, which share identical initial conditions. These simulations have been carried out in a box size of $205 h^{-1} \text{ Mpc}$, sufficient to capture large-scale modes relevant for our analysis. The full-physics simulation comprises an initial set of 2×2500^3 particles, half of which are dark matter with a mass resolution of $4.0 \times 10^7 h^{-1} M_\odot$, and the rest are gas tracer particles with an average cell mass of $7.4 \times 10^6 h^{-1} M_\odot$, the minimum gas softening length of 370 pc, and a physical softening length for dark matter equal to 1.48 kpc. The gravity-only simulation does not have the gas tracer particles, assuming baryons to be collisionless and to evolve only under the effect of gravity. The public data release provides 99 snapshots between $z = 20$ and $z = 0$.

The halo catalog is constructed using the friends-of-friends group-finding algorithm with subhalos identified with the SUBFIND algorithm [36, 37]. We use the bidirectional LHaloTree matching [38] to cross-identify halos between TNG300-1 and TNG300-1-Dark, with halos being considered a match if they share the FIRSTSUB Subhalo from the SUBFIND algorithm. An insignificant number of halos without matches ($\sim 3\%$) will be ignored for replacement in our analysis. The friends-of-friends halo finder is able to account for the asphericity in the distribution of matter, but can select halos which differ in their spherical overdensities in a concentration and mass dependent manner [39]. Given that baryonic effects can also change the halo triaxiality including the orientation, we decide to use spherical overdensity mass estimates in our analysis.

In our analysis, we will restrict ourselves to the $z = 0$ snapshot for simplicity, where baryonic feedback effects are most pronounced. We will only analyze halos with mass $M_{200m} \geq 10^{12} h^{-1} M_\odot$, encompassing galaxy- to cluster-scale halos, to focus on halos that are well resolved in simulations. We primarily focus on mass bins up to $10^{14.5} h^{-1} M_\odot$, as bins above this threshold contain very few halos.

3 Methodology

Our goal is to quantify the impact of baryonic effects on the matter distribution, specifically on the matter and galaxy–matter correlation functions. To directly assess this impact as a function of halo mass and radial extent, we construct a series of hybrid matter distributions by selectively replacing particles in halos of the TNG300-1-Dark simulation with their counterparts from the full-physics TNG300-1 run.

3.1 Isolating baryonic effects by halo mass

We consider halos in logarithmically spaced mass bins spanning $\log_{10}(M_{200m}/h^{-1} M_\odot) \in [12, 14.5]$. The use of spherical overdensity (SO) halos enables particle replacement within equal-volume regions in the gravity-only simulation, avoiding complications arising from potential shape mismatches between corresponding halos in the two runs. Because the centers of

matched halos do not coincide exactly between the simulations, replacements are performed relative to the assigned halo center in each matched pair.

For each mass bin, we identify matched halos between the full-physics and gravity-only simulations using the subhalo matching method outlined in section 2, ignoring for replacement any halo with no clear match. Around the center of each matched halo, we define a spherical replacement region of radius $R = \alpha R_{200m}$, where $\alpha \in [0.5, 1.0, 1.5, 2.0]$. Within this region, we replace all particles in the gravity-only simulation with those from the full-physics simulation—including dark matter, gas, stars, and black holes—while preserving both particle positions relative to the halo center and individual particle masses. To avoid double counting, we do not replace particles in smaller halos whose replacement regions overlap with those of more massive halos that are also being substituted. This is equivalent to adopting a hard halo exclusion scheme, where halos are not allowed to overlap.

For small replacement radii, $\alpha \in [0.5, 1.0]$, at most 5% of halos are excluded in any combination of mass bins. With larger replacement radii, $\alpha \in [1.5, 2.0]$, exclusion is more significant, on the order of 10% for most mass bin combinations, and $\sim 20\%$ for the case when all bins are replaced. While it may seem that many particles are being ignored in this scheme, most of these exclusions occur because one halo hosts another, especially when several mass bins are replaced at once. Exclusion does not affect the replacement of these particles that are shared by the halos, so only in edge cases of partial overlap there could be some particles which have not been replaced.

Hard exclusion likely leads to a small underestimate in the matter power suppression for large replacement radii. However this is necessary to avoid more complications. For example, halo centers are often offset between the full-physics and gravity-only simulations, requiring that particle locations be offset by the same amount, however, if a particle is shared by multiple halos, choosing its parent arbitrarily decides its offset and will result in artificial gaps or clumps in the distribution of particles at the boundary between halos.

A further complication arises because matched halos in the full-physics and gravity-only simulations may not have identical M_{200m} values or enclosed masses within the replacement radius, owing to baryon-driven mass redistribution. Simply replacing regions with lower total mass can introduce a spurious increase in the large-scale correlation amplitude. This occurs because a reduction in enclosed mass leads to fewer total particles in the box and hence fewer random pairs at larger separations, artificially boosting the correlation on large scales. This effect, typically at the few-percent level, is most pronounced for smaller replacement radii ($\alpha \in [0.5, 1.0]$) and diminishes for larger α . We enforce mass conservation on a halo-by-halo basis, uniformly redistributing the difference in mass incurred by replacement to the surrounding gravity-only simulation particles in a spherical region out to two times the replacement radius. This physically motivated approach conserves each halo mass (and global mass) and mimics the physical reality of baryonic effects ejecting mass to larger scales. We explore this method and alternatives in Appendix A, and demonstrate that enforcing mass conservation successfully removes the spurious large-scale signal. Important to note is that the relative contribution of each halo mass bin to suppression is entirely unchanged by this mass conservation method.

The procedure described above produces a modified simulation snapshot in which only halos within a specified mass bin contain matter redistributed by baryonic feedback, while the remainder of the volume evolves according to gravity alone. This construction enables us to isolate the contribution of baryonic effects as a function of both halo mass and radial distance from the halo center.

3.2 Measurements of the matter power spectrum

To quantify the suppression induced by baryonic feedback for a given halo mass bin, we compute the matter power spectrum of each modified snapshot using the Fast Fourier Transform (FFT) algorithm implemented in NBODYKIT [40], weighting by particle mass. We evaluate all unique combinations of halo mass bins and α values, as well as all pairwise combinations of two different mass bins and α , to identify how interactions between halos of different masses contribute to changes in the matter power spectrum.

We compute the power spectrum up to a wavenumber of $k = 31.32 h \text{Mpc}^{-1}$, using an FFT mesh of size $N_{\text{mesh}} = 512^3$ and utilizing the 'self-folding' technique outlined in [41]. The folding method allows for efficient small-scale power spectrum measurements by mapping the box on onto a factor f_{fold} subdivision of itself, essentially accomplishing the same thing as a finer mesh, but at significantly smaller computational memory footprint. We use two foldings of $f_{\text{fold}} = 2$ and $f_{\text{fold}} = 4$, where $f_{\text{fold}} = 2$ covers the power spectrum from $k \sim 8 h \text{Mpc}^{-1}$ to $k \sim 16 h \text{Mpc}^{-1}$, and $f_{\text{fold}} = 4$ covers $k \sim 16 h \text{Mpc}^{-1}$ to $k \sim 32 h \text{Mpc}^{-1}$. We use two foldings because each extra fold adds more noise to the measurement, so we only include regions where folding extends beyond the k limit of the previous folding to minimize the presence of this noise. Higher precision can be obtained with a finer mesh, but it is not necessary for our analysis.

While IllustrisTNG enables the power spectrum to be computed to much smaller scales ($k \sim 125 h \text{Mpc}^{-1}$) [29], we include only the range most relevant for weak lensing analysis. At this scale, we are able to measure the point of maximum suppression before baryonic feedback effects are dominated by processes within halos that boost matter power.

4 Results

4.1 Halo mass and radial dependence of the baryonic feedback

In this section, we quantify the suppression of the matter power spectrum for each replacement configuration by evaluating the ratio P/P_{GO} , where P denotes the power spectrum of the modified hybrid matter distribution and P_{GO} corresponds to that from the gravity-only simulation. The three panels of Fig. 1 illustrate results for different replacement radii: the left panel shows $\alpha = 0.5$, the middle shows $\alpha = 1.0$, and the right panel shows $\alpha = 2$. In each panel, the solid black line represents the total suppression of the matter power spectrum, calculated as the ratio of the full-physics to gravity-only power spectra.

On large scales ($k < 2 h \text{Mpc}^{-1}$), the two power spectra agree to better than one percent, indicating that baryonic effects have minimal impact in this regime. At intermediate scales ($k \in [3, 20] h \text{Mpc}^{-1}$), we observe a steady suppression of power reaching up to $\sim 20\%$, consistent with the expected influence of baryonic feedback processes. At smaller scales, the suppression plateaus and is followed by a mild upturn in power, reflecting the increasing dominance of baryonic contraction and star formation within halo cores.

When particles from halos with $M_{200m} > 10^{12} h^{-1} M_{\odot}$ in the gravity-only simulation are replaced with those from the full-physics simulation within a region extending to αR_{200m} , we obtain the grey curve in Fig. 1. The redistribution of matter within these halos produces a pronounced suppression in the matter power spectrum. For all α , the modification accounts for more than 90% of the total suppression observed in the full-physics simulation. The remaining contribution likely arises from lower-mass halos and from diffuse gas residing beyond the nominal halo boundaries.

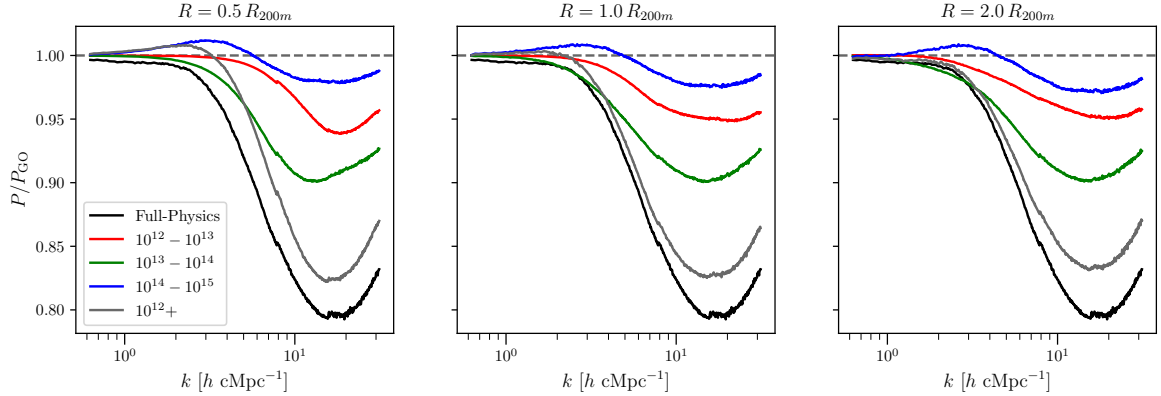


Figure 1: The ratio of the full-physics and gravity-only power spectrum P/P_{GO} for each non-overlapping one-dex mass bin. The three panels show three different replacement radii, i.e. the radii out to which matter is redistributed due to baryonic feedback. The gray curve is the power spectrum ratio for the case where all halos above $10^{12}h^{-1}M_{\odot}$ are replaced at once. The black curve is the ratio for the power spectrum computed on the entire full-physics simulation.

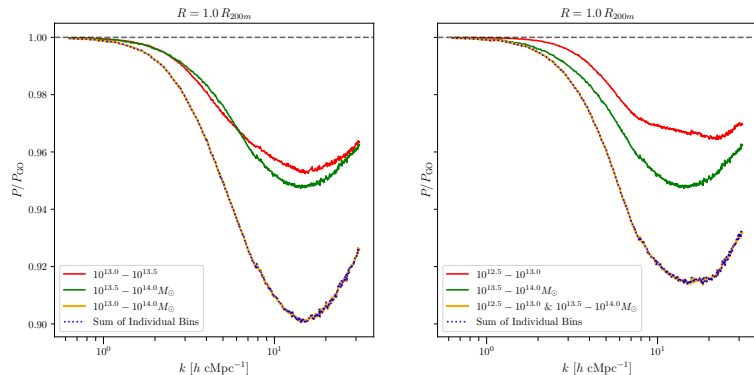


Figure 2: Left: The summation of the power spectrum ratio P/P_{GO} for two adjacent half-dex halo mass bins compared to the power spectrum computed from joint replacement of the two bins. **Right:** The same, but for two non-adjacent half-dex bins. The dotted blue curve is the sum of the red and green curves, and the solid orange curve is from the power spectrum computed with both half-dex bins replaced at once. The two curves are nearly identical in both cases, indicating that there are no significant cross-correlations between mass bins

To further disentangle the relative contributions by halo mass, we divide the sample into three logarithmic mass bins of $\log_{10}(M_{200m}/h^{-1}M_{\odot})$, as shown in Fig. 1. The red, green, and blue solid curves correspond to halos in the ranges [12, 13], [13, 14], and [14, 15], respectively. Low-mass halos ([12, 13]) are numerous and possess relatively shallow potential wells. The redistribution of matter within these systems produces a moderate suppression of around 5% in the total matter power spectrum. At the high-mass end ([14, 15]), halos can host powerful AGN capable of driving large-scale outflows, yet their rarity and their deeper potential wells limits their overall contribution, leading to a modest suppression of only about a couple of percent.

$\log_{10}(M_{200m})$	Radius	$0.5R_{200m}$	$1R_{200m}$	$1.5R_{200m}$	$2R_{200m}$
12 – 12.5		2.2	1.7	1.7	1.6
12.5 – 13		4.3	3.6	3.5	3.4
13 – 13.5		4.9	4.8	4.8	4.8
13.5 – 14		5.1	5.3	5.4	5.5
14 – 14.5		2.3	2.6	2.7	2.9
12-13	6.2	5.2	5.1	5.0	
12.5 – 13.5		9.0	8.1	8.1	7.9
13-14	9.9	10.0	10.0	9.9	
13.5 – 14.5		7.3	7.8	7.8	8.0
14-15	2.2	2.5	2.7	3.0	
12 – 12.5 & 13 – 13.5		6.4	6.4	6.3	6.2
12 – 12.5 & 13.5 – 14		6.8	6.9	6.9	6.9
12 – 12.5 & 14 – 14.5		4.4	4.2	4.3	4.4
12.5 – 13 & 13.5 – 14		9.3	8.6	8.7	8.7
12.5 – 13 & 14 – 14.5		6.6	6.0	6.1	6.2
13 – 13.5 & 14 – 14.5		7.0	7.3	7.3	7.5
12+	17.8	17.5	17.3	16.9	

Table 1: The maximum suppression percentage for each combination of mass bin and replacement radius. The table has been separated into half-dex bins, one-dex bins, and non-adjacent half-dex bins. In **bold** are the combinations plotted in figure 1. Also included is the case where all halos above $10^{12}h^{-1}M_{\odot}$ are replaced. The maximum suppression percentage of the entire full-physics simulation is 20.7%

The dominant effect arises from group-scale halos with $\log_{10}(M_{200m}/h^{-1}M_{\odot}) \in [13, 14]$, which produce a significantly larger suppression of $\sim 10\%$. This mass range accounts for $\sim 60\%$ of the total suppression attributed to baryonic redistribution in halos above $10^{12}h^{-1}M_{\odot}$. These results highlight the crucial role of feedback processes operating in group-scale halos and its large influence on the matter distribution relevant for interpretation of the cosmic shear.

The halo mass dependence of the impact of the baryonic effects seems to be consistent with the predominance of the fraction of total matter present in different halo mass bins. This can be computed as

$$f(M_1, M_2) = \frac{1}{\bar{\rho}} \int_{M_1}^{M_2} dM n(M) M \quad (4.1)$$

where $n(M)dM$ is the halo mass function and represents the number density of halos between $[M, M + dM]$, and $\bar{\rho}$ is the average matter density of the Universe. These mass fractions are 7.8 percent, 8.4 percent and 4.3 percent in the mass bins [12, 13], [13, 14] and [14, 15],

respectively. The effect is thus largest in the mass bin which contributes most to the mass fraction.

To investigate the radial dependence of baryonic feedback effects, we compare the suppression curves across the three panels of Fig. 1. For group-scale halos, replacing matter within the radial range $[0.5, 2]R_{200m}$ produces little additional impact on the matter power spectrum. This behavior likely reflects the balance between feedback energetics and the depth of the gravitational potential wells in these systems, which restrict the redistribution of matter beyond the halo boundary.

Halos with $\log_{10}(M_{200m}/h^{-1}M_{\odot}) > 14$ show a small increase ($\sim 1\%$) in the suppression of the matter power spectrum when replaced out to larger scales. This result likely indicates that AGN feedback in these high-mass systems is able to overcome the deeper potential well and eject matter out to larger distances, such that including these extant regions still has a suppressive effect on the matter power spectrum. These halos also show a consistent relative boost in the power spectrum at $k \sim 2 - 4 h \text{ Mpc}^{-1}$, likely a result of baryonic condensation and dark matter contraction in the inner regions of these halos, which increase the central densities and thus enhance power on intermediate scales corresponding to the one-halo term.

In contrast, halos with $\log_{10}(M_{200m}/h^{-1}M_{\odot}) < 13$ exhibit a decrease in the contribution to suppression (a few percent) when replaced out to larger radii. In these halos, stellar feedback processes such as supernovae and stellar winds can dominate AGN feedback, so this result may be due to these processes only ejecting gas to modest distances. It is also possible that replacing out to larger radii includes gas that has fallen back into the halo, or even matter from other nearby halos in the case that the halo exists within a group or cluster. The exact amount of the change is dependent upon the exact manner or radius out to which we increase the mass in gravity-only simulation particles. In any case, it seems that the suppressive effects are concentrated in the central region of these halos.

It is worth noting again that our exclusion of halos outlined in section 3 likely results in underestimates of suppression for large replacement radii. This is especially true for galaxy-scale halos that have significant populations in groups or clusters, meaning that our strict exclusion will eliminate a non-negligible amount of halos that only partially overlap in these cases. This will result in an underestimate that may dominate any increase in suppression from extending to larger scales.

As a quantitative summary, we calculate the maximum suppression percentage for each combination of mass bin and replacement radius—corresponding to the minimum of the P/P_{GO} ratio shown in Fig. 1. These suppression values, including those for intermediate half-dex mass bins, are reported in Table 1.

Interestingly we find that the total suppression of matter distribution compared to the gravity-only case can be simply obtained as a sum of the suppressions from two individual mass bins. In Fig. 2, we demonstrate that the total suppression of the matter power spectrum can be accurately reconstructed by summing the contributions from individual halo mass bins, both for adjacent and non-adjacent mass bins. The solid red and green curves show the suppression measured for halos within two different half-dex mass bins, $M_{200m}/h^{-1}M_{\odot} \in [13.0, 13.5]$ and $[13.5, 14.0]$ respectively for the adjacent case and $M_{200m}/h^{-1}M_{\odot} \in [12.5, 13.0]$ and $[13.5, 14]$ respectively for the non-adjacent case. The orange curves shows the resulting suppression from a simultaneous replacement. The dashed blue curves shows the cumulative suppression obtained by simply adding the suppression effects from the two mass bins.

The close agreement between the two confirms that the overall suppression is approx-

imately additive across halo mass bins. This behavior indicates that the baryonic redistribution in halos of different masses acts largely independently, with minimal cross-coupling between mass scales. Consequently, the total baryonic impact on the matter power spectrum can be understood as the superposition of the effects contributed by distinct halo populations.

4.2 Impact on the group-galaxy weak lensing signal

Given that our results indicate a non-monotonic dependence of baryonic effects on halo mass in the total matter power spectrum, we next ask whether this behavior can serve as an observable signature of baryonic feedback. To explore this, we turn to the cross-correlation of matter with halos of different masses as probed by the galaxy–galaxy (or group–galaxy) lensing signal. Baryonic feedback processes are expected to modify this weak lensing signal, $\Delta\Sigma(R)$, through the redistribution of matter around halos.

The excess surface density is defined as

$$\Delta\Sigma = \bar{\Sigma}(< R) - \langle \Sigma(R) \rangle, \quad (4.2)$$

where $\bar{\Sigma}(< R)$ is the mean projected surface density within a projected radius R from the halo center, and $\langle \Sigma(R) \rangle$ is the azimuthally averaged surface density at that same distance. The corresponding observable in weak lensing measurements is the mean tangential shear of background galaxies, γ_t , which relates to $\Delta\Sigma$ via

$$\gamma_t = \frac{\Delta\Sigma}{\Sigma_{\text{crit}}}. \quad (4.3)$$

Here, Σ_{crit} is the critical surface density, which depends on the geometry of the lensing configuration and thus on the redshifts of both lenses and sources. The critical surface density is given by

$$\Sigma_{\text{crit}} = \frac{c^2}{4\pi G} \frac{D_s}{D_l D_{ls}} \frac{1}{(1+z_l)^2}, \quad (4.4)$$

where D_s , D_l , and D_{ls} are the angular diameter distances to the source, to the lens, and from the lens to the source, respectively. On the angular scales relevant to our analysis, the uncertainty in γ_t is dominated by the intrinsic ellipticity of galaxies (the so-called shape noise).

We project the three-dimensional matter density along the line of sight toward the halos and compute $\Delta\Sigma(R)$ for the same halo mass bins used in our matter power spectrum analysis. This yields predictions for the weak lensing signal in both the full-physics and gravity-only simulations. We then quantify the impact of baryonic feedback by comparing the stacked $\Delta\Sigma(R)$ profiles of matched halos between the two simulations. Errors on these measurements are estimated assuming the depth and source density of a DES-like survey. The sample variance in each mass bin is computed via jackknife resampling, while the shape noise is estimated using

$$\sigma_{\Delta\Sigma} = \Sigma_{\text{crit}} \frac{\sigma_\varepsilon}{\sqrt{N_{\text{lenses}} n \Omega}}, \quad (4.5)$$

where $\sigma_\varepsilon = 0.25$ is the root-mean-square intrinsic ellipticity per galaxy [42], N_{lenses} is the number of lensing halos in a given mass bin, $n = 4.2 \text{ galaxies arcmin}^{-2}$ is the surface density of background source galaxies, and Ω denotes the solid angle of the annulus within which the

tangential shears are averaged. The factor $N_{\text{lenses}}n\Omega$ therefore represents the total number of lens–source pairs contributing to the measurement in each radial bin.

To emulate realistic survey conditions, we assume source galaxies distributed over $z_s \in [0.5, 1.0]$ and lens halos over $z_l \in [0.2, 0.4]$, consistent with analyses using MAGLIM lenses and DES source galaxies [42, 43]. The number of lenses in each mass bin is derived from their number density in the IllustrisTNG simulation, scaled to match the comoving volume probed by DES in this redshift range. This implicitly assumes that all central galaxies in halos within this mass range are observable at such low redshifts, a reasonable approximation given the survey depth of DES.

The resulting $\Delta\Sigma(R)$ profiles are shown in Figure 3. The left-hand panel displays the net lensing signal of baryons, combining the contributions from gas, stars, and black holes, for each halo mass bin. The distinct shapes of these profiles highlight the deviations of the baryonic components from the underlying matter distribution in the collisionless simulation.

In the middle panel, we compare the total weak lensing signal in the full-physics simulation to that in the gravity-only run. The error bars represent the combined contribution from sample variance and shape noise. This comparison isolates the impact of baryonic feedback processes on the matter distribution. Within the inner regions of halos, the baryonic profiles follow approximately $\Delta\Sigma(R) \propto R^{-1}$, consistent with near isothermal profiles for baryons. At larger radii, the profiles steepen towards $\Delta\Sigma(R) \propto R^{-2}$, reflecting the transition to the outskirts where feedback-driven redistribution of matter becomes relatively insignificant.

The left-hand panel shows the relative difference between the weak lensing profiles in the full-physics and gravity-only simulations. For the lowest-mass halos, baryonic condensation in the central regions enhances the lensing signal at scales below $\sim 0.2R_{\text{vir}}$. Beyond this radius, however, the signal becomes suppressed relative to the collisionless case due to feedback-driven mass redistribution. As halo mass increases, this central enhancement diminishes, and the maximum suppression is observed for group-scale halos with $\log M_{200m} \in [13, 14]$. At even higher masses, the suppression weakens again, consistent with the deeper potential wells that limit baryonic outflows. Beyond the virial radius, the full-physics and collisionless profiles converge, indicating that baryonic effects are confined largely within a few halo radii.

These results demonstrate that the suppression of the matter power spectrum seen in the full-physics simulation has a clear counterpart in the weak lensing signal. In particular, the scale-dependent deviations in $\Delta\Sigma(R)$ encode the same redistribution of matter responsible for the power spectrum suppression. This suggests that baryonic feedback can be effectively probed through weak lensing measurements, especially when analyzed as a function of halo mass. While an exact division of halos into narrow mass bins is challenging in observational data, practical alternatives exist. For instance, one can stack halos in bins of group luminosity, exploiting the strong correlation between total luminosity and halo mass. Abundance matching with cosmological simulations can then be used to calibrate these luminosity bins to their corresponding halo masses, allowing for an observational test of the mass-dependent baryonic effects predicted here. Another option is to use the 1-halo term of the measured weak lensing signal to get the estimate of the mass of the halo directly and study the redistribution of matter within halo of given mass. Both options have pros and cons. While the former approach relies on the intermediate group properties and abundance matching, it will be able to measure both shape and amplitude change in the density profile. The latter does not involve going through abundance matching and is a more direct observational probe, although that will only be able to probe the change in the shape of the density profile.

We note that [17] found that IllustrisTNG systematically underestimates baryonic feed-

back effects compared to what is observed in kSZ selected clusters. This points towards potentially even stronger deviation from the gravity-only weak lensing signal at small scales, and some of the conclusions may depend upon the exact implementation. However, the deviation of the weak lensing profiles from expectations from collisionless simulations can be a useful probe of the baryonic effects and distinguish it from changes in cosmology.

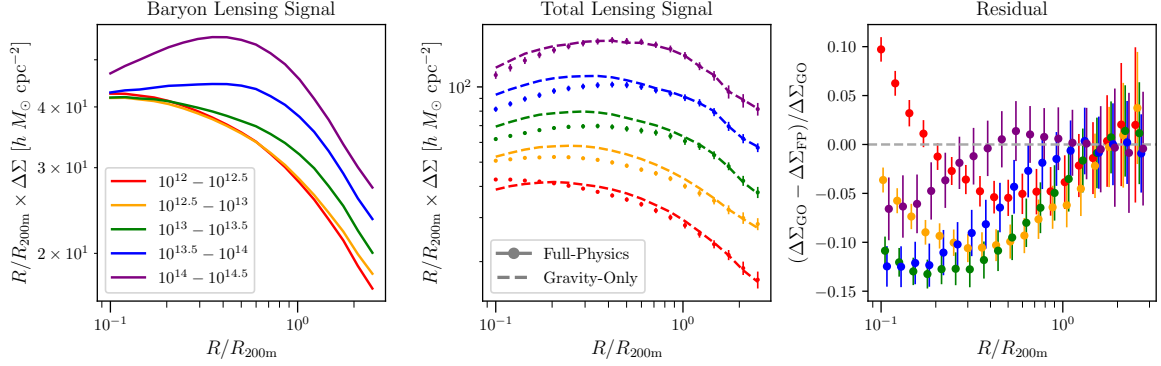


Figure 3: **Left:** The mean weak lensing signal profile of baryons for each mass bin, i.e. the sum of the gas, star, and black hole lensing signals. **Center:** The total lensing profiles for each halo mass bin from the full-physics case with estimated shape noise and sampling error mimicking a DES-like survey, plotted alongside the lensing profiles from the gravity-only simulation. Note that these first two plots are multiplied by R/R_{200m} for visual clarity. **Right:** The residual profile, i.e. the difference between the gravity-only and full-physics weak lensing signals divided by the gravity-only signal for each mass bin.

5 Summary and Discussion

In this work, we have developed and applied a hybrid simulation framework to quantify the impact of baryonic feedback on the matter distribution using the IllustrisTNG simulations. By selectively replacing particles in the collisionless TNG300-1-Dark simulation with their full-physics counterparts as a function of halo mass and radial extent, we isolated how baryonic processes modify structure formation across different mass scales. Our key results can be summarized as follows:

- We constructed controlled realizations of the matter field by replacing particles within spherical regions of radius αR_{200m} around halos in different mass bins and matched between the full-physics and gravity-only simulations. Variations in the halo mass bins and α allowed us to study the mass and radial dependence of the baryonic effects on the matter power spectrum.
- Nearly 90 percent of the total suppression of the matter power spectrum in the full-physics simulation, which reaches up to 20% at $k \sim 10 h \text{ Mpc}^{-1}$, can be explained due to feedback from halos with masses $\log M_{200m} > 12$.
- Group-scale halos ($\log M_{200m} \in [13, 14]$) contribute the dominant ~ 10 percent suppression, representing 60 percent of the total effect from all halos above $\log M_{200m} = 12$. Lower-mass halos ($\log M_{200m} \in [12, 13]$) and cluster-scale halos ($\log M_{200m} > 14$) each

contribute only a few percent to the total suppression. The effect is non-monotonic with halo mass, it peaks at group scales, consistent with efficient AGN feedback redistributing matter beyond the virial radius.

- We demonstrated that the suppression from different halo mass bins adds linearly, demonstrating that baryonic feedback operates as a near-independent contribution from each mass scale.
- Effects of feedback on the matter power spectrum can be simply explained by redistribution of matter within R_{200m} and redistributing some fraction of this mass expelled by the feedback effects into the surrounding volume at a distance about 1.5 times larger.
- The differential surface density profiles, $\Delta\Sigma(R)$, from the full-physics simulation show enhanced central signals at low masses and suppressed signals at larger radii, mirroring the redistribution seen in the power spectrum. The maximum suppression in $\Delta\Sigma$ occurs for group-scale halos, again highlighting its importance in baryonic feedback.

Our results suggest that mass-dependent weak lensing measurements, particularly when stacking by group luminosity or richness, can directly probe baryonic feedback signatures. The distinct non-monotonic dependence of suppression on halo mass provides a potential observational discriminator of feedback models. Although seemingly straightforward, some systematics are worth pointing out. Group finding algorithms often have trouble identifying isolated halos, and could either fragment groups, or combine them due to line-of-sight projection effects (see e.g., [44]). There are also potential issues related to the identification of central galaxies, as well as the mis-centering between central galaxies and the true potential centers of halos.

5.1 Connections to weak lensing and SZ measurements

We have shown that the suppression of the matter power spectrum directly translates into weak-lensing observables such as the cosmic shear power spectrum and the galaxy-group lensing signal [3, 45]. Our results therefore underscore the need to model the halo mass dependence of baryonic feedback in future weak lensing analyses. While current 3×2 -point analyses often exclude small scales due to feedback-related uncertainties [46], properly incorporating these scales, using physically motivated models or simulation-based calibrations, could recover a significant amount of cosmological information currently discarded [8, 18, 19, 47].

The peak contribution to cosmic shear occurs at $z \simeq 0.5$, somewhat higher than the redshift studied here. While our results at $z = 0$ capture the cumulative impact of baryonic processes, the redshift evolution of the suppression is expected to be mild for $z \lesssim 1$ and $k \lesssim 10, h, \text{Mpc}^{-1}$ [48]. Nonetheless, the joint dependence of feedback on halo mass, spatial scale, and cosmic time remains an open question that future simulations and tomographic weak lensing analyses could address.

Complementary probes of baryonic feedback are emerging from observations of the thermal and kinetic Sunyaev–Zel’dovich (tSZ and kSZ) effects in groups and clusters [16, 17, 20, 49, 50]. These measurements directly trace the thermodynamic state of the gas, providing independent constraints on the redistribution of baryons within and around halos. The group-mass regime, which our work has identified here as most influential for the matter power suppression, is also the most accessible to current kSZ and weak lensing measurements. While most SZ observations were limited to relatively massive systems, recently stacked SZ–lensing

analyses have been shown to extend sensitivity to lower masses, modulo uncertainties in the halo–observable relation [20, 51, 52]. Forthcoming high-sensitivity CMB experiments, such as the Simons Observatory [53], promise to probe baryonic feedback across a broader halo mass range and provide crucial constraints on the rearrangement of matter in the Universe.

Finally, while baryonic probes such as X-ray and SZ measurements are directly sensitive to the baryonic gas, we emphasize that the total matter distribution, i.e., baryons and the dark matter, is jointly rearranged by feedback. This redistribution alters the gravitational potential and thus affects cosmological observables even where baryons themselves are sub-dominant. Surveys such as the Rubin LSST which will start imminently will increase the surveyed area compared to the Dark Energy Survey by a factor of 4, and the better depth will lead to an increase in the number of galaxies per square arcmin of at least 3. This will significantly reduce the statistical error on the cosmic shear measurements down to small scales, as well as the group galaxy lensing signals. Together with the exquisite angular resolution and depth provided by space based surveys such as Euclid and Roman, the quality and quantity of data will increase dramatically in the near future. To realize the scientific output of these surveys to the fullest, joint interpretation of future high-precision weak lensing, X-ray and SZ data will therefore require models that capture both the baryonic and the induced dark matter response to feedback.

5.2 Improving Theoretical Models

The results presented here demonstrate that baryonic feedback produces a non-monotonic and mass-dependent impact on both the matter distribution within halos and the total matter power spectrum. This complexity highlights a key challenge for cosmological inference: baryonic correction models and emulators should not just be tuned to reproduce the total matter power spectrum. Our findings show that baryonic feedback reshapes the internal structure and outskirts of halos in a mass-dependent manner. Accurately capturing this may require a new generation of emulators capable of jointly predicting the halo–matter connection and the corresponding large-scale matter correlation in a self-consistent framework.

Emulators such as DARKEMULATOR [54] and BACCOEMU [55] provide predictions of nonlinear clustering and halo statistics, but do not include both small scales and halo matter cross correlations in the presence of baryonic effects. Hybrid emulators which can parameterize the mass dependent redistribution of matter within halos such as HMx [13] or the baryonification project [14] which could be adapted to self-consistently predict the halo matter cross-correlations and the impact on the matter power spectrum are promising ways forward.

Acknowledgements

We would like to thank Sunao Sugiyama, Shivam Pandey, and Shreya Mukherjee for the helpful feedback and discussions, and Dylan Nelson for his help in providing access to the Illustris TNG simulation and the python notebook server close to the data. KM would like to thank IUCAA for its hospitality during his visit to India where a large fraction of this research work was conducted.

The IllustrisTNG simulations were undertaken with compute time awarded by the Gauss Centre for Supercomputing (GCS) under GCS Large-Scale Projects GCS-ILLU and GCS-DWAR on the GCS share of the supercomputer Hazel Hen at the High Performance Com-

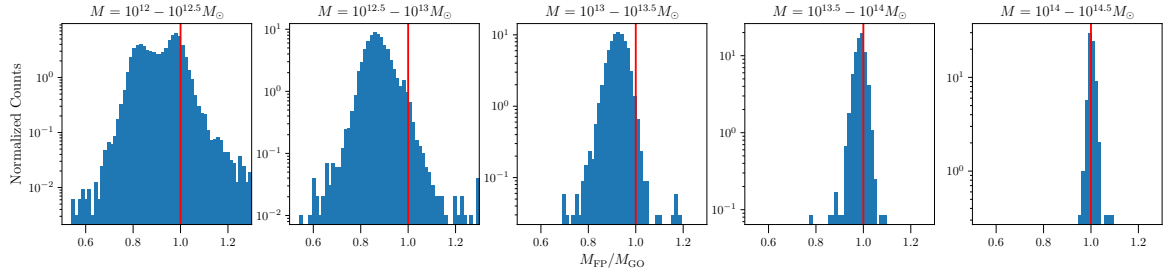


Figure 4: The histogram of mass ratios between corresponding halos in the full-physics and gravity-only simulations. Full-physics halos are seen to generally have a slightly lower M_{200m} relative to their gravity-only simulation counterparts because baryonic feedback processes eject gas ejected out beyond R_{200m} .

puting Center Stuttgart (HLRS), as well as on the machines of the Max Planck Computing and Data Facility (MPCDF) in Garching, Germany.

A Mass Conservation

We replace matter in the gravity-only simulation with that from the full-physics simulation. When halos are matched between the two, we find that the total replaced mass does not exactly equal the original mass in the gravity-only case. This difference is expected as baryonic feedback processes such as AGN activity and supernovae eject gas to large radii, while gas cooling and galaxy formation pull matter inward. Consequently, the mass enclosed within a fixed spherical radius around a halo center differs between the two simulations. Typically, full-physics halos contain less mass than their gravity-only counterparts, except at the highest halo masses where deeper potential wells retain more baryons. This trend is evident in Fig. 4, which shows the ratio of M_{200m} between the matched halos.

When halo particles are replaced within a fixed multiple of R_{200m} , the result is generally a modest reduction in total halo mass. Summed over the full volume, these losses correspond to a global mass deficit of order $\sim 1\%$. While this reduction is physically meaningful, if unaccounted for, it can introduce a spurious boost in large-scale power, as seen in the dashed curves of Fig. 5. The effect is strongest for the lowest halo mass bins ($M_{200m} \in [10^{12}, 10^{13}] M_{\odot}$) and for small replacement radii ($\alpha \in [0.5, 1.0]$). At larger radii or when replacing more massive halos, the boost becomes negligible because the replaced regions encompass more of the baryon-rich outskirts expelled by feedback, reducing the net mass deficit. Physically, the loss of mass on small scales lowers the local overdensity contrast and redistributes power into larger-scale modes, thereby producing the apparent increase in large-scale clustering amplitude.

We implement and compare two complementary methods of enforcing mass conservation, both of which successfully eliminate the spurious large-scale power boosts, but differ in their impact on small-scale structure. In the first approach, we locally rescale the masses of replaced particles within each halo by a factor of $M_{GO}(< R)/M_{FP}(< R)$, where $M_{GO}(< R)$ and $M_{FP}(< R)$ are the enclosed masses within the replacement radius in the gravity-only and full-physics simulations, respectively. This results in a mere change in the normalized density profile of a halo, and ensures that each halo retains its original mass after replacement. Such replacement removes the large-scale boost (see dashed lines in Fig. 5). However,

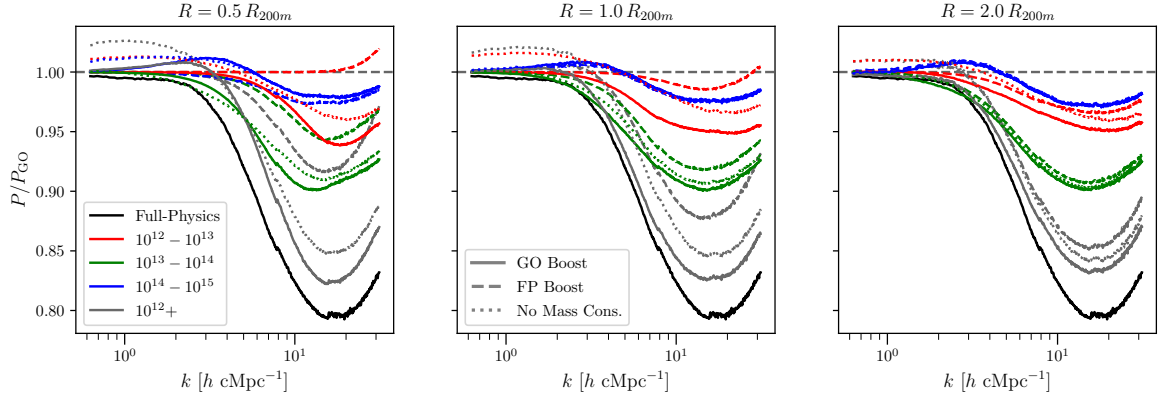


Figure 5: P/P_{GO} for each non-overlapping one-dex mass bin for three different mass conservation methods. Solid curves correspond to halo-by-halo redistribution of the mass deficit to surrounding gravity-only simulation particles. Dashed curves correspond to halo-by-halo boosting of the replaced full-physics particles. Dotted curves correspond to no mass conservation at all.

the rescaling also counteracts the very baryonic effects we aim to capture, i.e., the expulsion of matter from halo interiors to larger radii. As a result, the small-scale suppression in the power spectrum is artificially underestimated. Although some residual suppression remains due to the altered spatial distribution of particles, this method does not fully represent the physical redistribution of baryons.

Our second, more physically motivated approach conserves both halo and global mass by redistributing the missing mass to the gravity-only particles surrounding each halo, rather than rescaling particles inside the replacement region. Specifically, the mass deficit is distributed uniformly among gravity-only particles within a spherical shell extending from R_{replace} to $2R_{\text{replace}}$. This mimics the baryonic feedback process, where ejected material populates the outskirts of halos. This approach also removes the large-scale boost, but results in a somewhat stronger small-scale suppression than the local rescaling method. This enhancement is physically plausible, as baryonic feedback indeed transfers mass from the halo interior to outer regions, lowering central densities. By distributing mass outward rather than scaling it up, this scheme preserves the qualitative effect of feedback while enabling a controlled study of how different radial ranges contribute to the total suppression of the matter power spectrum (see solid lines in Fig. 5). We have experimented with various factors out to which we redistribute the mass, and find our conclusions robust to our fiducial choice.

References

- [1] J.F. Acevedo, H. An, Y. Boukhtouchen, J. Bramante, M.L.A. Richardson and L. Sansom, *Dark matter induced baryonic feedback in galaxies*, [Phys. Rev. D](#) **110** (2024) 083004.
- [2] P. Biernacki and R. Teyssier, *The combined effect of agn and supernovae feedback in launching massive molecular outflows in high-redshift galaxies*, [Monthly Notices of the Royal Astronomical Society](#) **475** (2018) 5688–5703.
- [3] N.E. Chisari, A.J. Mead, S. Joudaki, P.G. Ferreira, A. Schneider, J. Mohr et al., *Modelling baryonic feedback for survey cosmology*, [The Open Journal of Astrophysics](#) **2** (2019) .

- [4] M. Gebhardt, D. Anglés-Alcázar, J. Borrow, S. Genel, F. Villaescusa-Navarro, Y. Ni et al., *Cosmological baryon spread and impact on matter clustering in camels*, 2023.
- [5] J. Schaye, R.A. Crain, R.G. Bower, M. Furlong, M. Schaller, T. Theuns et al., *The eagle project: simulating the evolution and assembly of galaxies and their environments*, *Monthly Notices of the Royal Astronomical Society* **446** (2014) 521–554.
- [6] A. Nicola, F. Villaescusa-Navarro, D.N. Spergel, J. Dunkley, D. Anglés-Alcázar, R. Davé et al., *Breaking baryon-cosmology degeneracy with the electron density power spectrum*, *Journal of Cosmology and Astroparticle Physics* **2022** (2022) 046.
- [7] S. Pandey, J.C. Hill, A. Alarcon, O. Alves, A. Amon, D. Anbajagane et al., *Constraints on cosmology and baryonic feedback with joint analysis of dark energy survey year 3 lensing data and act dr6 thermal sunyaev-zel'dovich effect observations*, 2025.
- [8] A. Chen, G. Aricò, D. Huterer, R.E. Angulo, N. Weaverdyck, O. Friedrich et al., *Constraining the baryonic feedback with cosmic shear using the des year-3 small-scale measurements*, *Monthly Notices of the Royal Astronomical Society* **518** (2022) 5340–5355.
- [9] E. Semboloni, H. Hoekstra, J. Schaye, M.P. van Daalen and I.G. McCarthy, *Quantifying the effect of baryon physics on weak lensing tomography: Baryon physics and weak lensing tomography*, *Monthly Notices of the Royal Astronomical Society* **417** (2011) 2020–2035.
- [10] A.R. Zentner, E. Semboloni, S. Dodelson, T. Eifler, E. Krause and A.P. Hearin, *Accounting for baryons in cosmological constraints from cosmic shear*, *Physical Review D* **87** (2013) .
- [11] A.R. Zentner, D.H. Rudd and W. Hu, *Self-calibration of tomographic weak lensing for the physics of baryons to constrain dark energy*, *Physical Review D* **77** (2008) .
- [12] E. Semboloni, H. Hoekstra and J. Schaye, *Effect of baryonic feedback on two- and three-point shear statistics: prospects for detection and improved modelling*, *Monthly Notices of the Royal Astronomical Society* **434** (2013) 148–162.
- [13] A.J. Mead, S. Brieden, T. Tröster and C. Heymans, *jscpzhmcode-2020jscpz: improved modelling of non-linear cosmological power spectra with baryonic feedback*, *Monthly Notices of the Royal Astronomical Society* **502** (2021) 1401–1422.
- [14] K. Osato and D. Nagai, *Baryon pasting algorithm: halo-based and particle-based pasting methods*, *Monthly Notices of the Royal Astronomical Society* **519** (2022) 2069–2082.
- [15] P.R. S., E. Krause, K. Dolag, K. Benabed, T. Eifler, E. Ayçoberry et al., *Impact of cosmology dependence of baryonic feedback in weak lensing*, 2024.
- [16] C.-H. To, S. Pandey, E. Krause, N. Dalal, D. Anbajagane and D.H. Weinberg, *Deciphering baryonic feedback with galaxy clusters*, 2024.
- [17] B. Hadzhiyska, S. Ferraro, B.R. Guachalla, E. Schaan, J. Aguilar, N. Battaglia et al., *Evidence for large baryonic feedback at low and intermediate redshifts from kinematic sunyaev-zel'dovich observations with act and desi photometric galaxies*, 2025.
- [18] H.-J. Huang, T. Eifler, R. Mandelbaum, G.M. Bernstein, A. Chen, A. Choi et al., *Dark energy survey year 1 results: Constraining baryonic physics in the universe*, *Monthly Notices of the Royal Astronomical Society* **502** (2021) 6010–6031.
- [19] A. Schneider, S.K. Giri, S. Amodeo and A. Refregier, *Constraining baryonic feedback and cosmology with weak-lensing, x-ray, and kinematic sunyaev-zeldovich observations*, *Monthly Notices of the Royal Astronomical Society* **514** (2022) 3802–3814.
- [20] L. Bigwood, A. Amon, A. Schneider, J. Salcido, I.G. McCarthy, C. Preston et al., *Weak lensing combined with the kinetic sunyaev zel'dovich effect: A study of baryonic feedback*, 2024.
- [21] J. Xu, T. Eifler, E. Krause, V. Miranda, J. Salcido and I. McCarthy, *Constraining baryonic feedback and cosmology from des y3 and planck pr4 6×2pt data. i. λ cdm models*, 2025.

[22] J. Siegel, A. Amon, I.G. McCarthy, L. Bigwood, M. Yamamoto, E. Bulbul et al., *Joint x-ray, kinetic sunyaev-zeldovich, and weak lensing measurements: toward a consensus picture of efficient gas expulsion from groups and clusters*, 2025.

[23] R. Terasawa, X. Li, M. Takada, T. Nishimichi, S. Tanaka, S. Sugiyama et al., *Exploring the baryonic effect signature in the hyper suprime-cam year 3 cosmic shear two-point correlations on small scales: the s_8 tension remains present*, 2024.

[24] K.P. Sarmiento, A. Lagu  , M. Madhavacheril, B. Jain and B. Sherwin, *Reconstructing the shape of the non-linear matter power spectrum using cmb lensing and cosmic shear*, 2025.

[25] D. Nelson, V. Springel, A. Pillepich, V. Rodriguez-Gomez, P. Torrey, S. Genel et al., *The IllustrisTNG simulations: public data release*, *Computational Astrophysics and Cosmology* **6** (2019) 2 [[1812.05609](#)].

[26] A. Pillepich, D. Nelson, L. Hernquist, V. Springel, R. Pakmor, P. Torrey et al., *First results from the IllustrisTNG simulations: the stellar mass content of groups and clusters of galaxies*, *Mon. Not. Roy. Astron. Soc.* **475** (2018) 648 [[1707.03406](#)].

[27] F. Marinacci, M. Vogelsberger, R. Pakmor, P. Torrey, V. Springel, L. Hernquist et al., *First results from the IllustrisTNG simulations: radio haloes and magnetic fields*, *Mon. Not. Roy. Astron. Soc.* **480** (2018) 5113 [[1707.03396](#)].

[28] J.P. Naiman, A. Pillepich, V. Springel, E. Ramirez-Ruiz, P. Torrey, M. Vogelsberger et al., *First results from the IllustrisTNG simulations: a tale of two elements - chemical evolution of magnesium and europium*, *Mon. Not. Roy. Astron. Soc.* **477** (2018) 1206 [[1707.03401](#)].

[29] V. Springel, R. Pakmor, A. Pillepich, R. Weinberger, D. Nelson, L. Hernquist et al., *First results from the IllustrisTNG simulations: matter and galaxy clustering*, *Mon. Not. Roy. Astron. Soc.* **475** (2018) 676 [[1707.03397](#)].

[30] M. Vogelsberger, S. Genel, V. Springel, P. Torrey, D. Sijacki, D. Xu et al., *Introducing the Illustris Project: simulating the coevolution of dark and visible matter in the Universe*, *Mon. Not. Roy. Astron. Soc.* **444** (2014) 1518 [[1405.2921](#)].

[31] S. Genel, M. Vogelsberger, V. Springel, D. Sijacki, D. Nelson, G. Snyder et al., *Introducing the Illustris project: the evolution of galaxy populations across cosmic time*, *Mon. Not. Roy. Astron. Soc.* **445** (2014) 175 [[1405.3749](#)].

[32] D. Sijacki, M. Vogelsberger, S. Genel, V. Springel, P. Torrey, G.F. Snyder et al., *The Illustris simulation: the evolving population of black holes across cosmic time*, *Mon. Not. Roy. Astron. Soc.* **452** (2015) 575 [[1408.6842](#)].

[33] M. Vogelsberger, S. Genel, V. Springel, P. Torrey, D. Sijacki, D. Xu et al., *Properties of galaxies reproduced by a hydrodynamic simulation*, *Nature* **509** (2014) 177 [[1405.1418](#)].

[34] V. Springel, *E pur si muove: Galilean-invariant cosmological hydrodynamical simulations on a moving mesh*, *Mon. Not. Roy. Astron. Soc.* **401** (2010) 791 [[0901.4107](#)].

[35] R. Weinberger, V. Springel and R. Pakmor, *The arepo public code release*, *The Astrophysical Journal Supplement Series* **248** (2020) 32.

[36] V. Springel, S.D.M. White, G. Tormen and G. Kauffmann, *Populating a cluster of galaxies - I. Results at $z=0$* , *Mon. Not. Roy. Astron. Soc.* **328** (2001) 726 [[astro-ph/0012055](#)].

[37] K. Dolag, S. Borgani, G. Murante and V. Springel, *Substructures in hydrodynamical cluster simulations*, *Mon. Not. Roy. Astron. Soc.* **399** (2009) 497 [[0808.3401](#)].

[38] D. Nelson, A. Pillepich, S. Genel, M. Vogelsberger, V. Springel, P. Torrey et al., *The *illustris* simulation: Public data release*, *Astronomy and Computing* **13** (2015) 12–37.

[39] S. More, F.C. van den Bosch, M. Cacciato, R. Skibba, H.J. Mo and X. Yang, *Satellite*

kinematics - iii. halo masses of central galaxies in sdss: Satellite kinematics - iii, Monthly Notices of the Royal Astronomical Society **410** (2010) 210–226.

- [40] N. Hand, Y. Feng, F. Beutler, Y. Li, C. Modi, U. Seljak et al., *Nbodykit: An open-source, massively parallel toolkit for large-scale structure*, *The Astronomical Journal* **156** (2018) 160.
- [41] A. Jenkins, C.S. Frenk, F.R. Pearce, P.A. Thomas, J.M. Colberg, S.D.M. White et al., *Evolution of structure in cold dark matter universes*, *The Astrophysical Journal* **499** (1998) 20–40.
- [42] A. Amon, D. Gruen, M. Troxel, N. MacCrann, S. Dodelson, A. Choi et al., *Dark energy survey year 3 results: Cosmology from cosmic shear and robustness to data calibration*, *Physical Review D* **105** (2022) .
- [43] J. Prat, J. Blazek, C. Sánchez, I. Tutusaus, S. Pandey, J. Elvin-Poole et al., *Dark energy survey year 3 results: High-precision measurement and modeling of galaxy-galaxy lensing*, *Physical Review D* **105** (2022) .
- [44] D.J.R. Campbell, C.M. Baugh, P.D. Mitchell, J.C. Helly, V. Gonzalez-Perez, C.G. Lacey et al., *A new methodology to test galaxy formation models using the dependence of clustering on stellar mass*, *Mon. Not. Roy. Astron. Soc.* **452** (2015) 852 [[1412.3804](#)].
- [45] N.E. Chisari, M.L.A. Richardson, J. Devriendt, Y. Dubois, A. Schneider, A.M.C. Le Brun et al., *The impact of baryons on the matter power spectrum from the horizon-agn cosmological hydrodynamical simulation*, *Monthly Notices of the Royal Astronomical Society* **480** (2018) 3962–3977.
- [46] L. Secco, S. Samuroff, E. Krause, B. Jain, J. Blazek, M. Raveri et al., *Dark energy survey year 3 results: Cosmology from cosmic shear and robustness to modeling uncertainty*, *Physical Review D* **105** (2022) .
- [47] G. Aricò, R.E. Angulo, M. Zennaro, S. Contreras, A. Chen and C. Hernández-Monteagudo, *Des y³ cosmic shear down to small scales: Constraints on cosmology and baryons*, *Astronomy & Astrophysics* **678** (2023) A109.
- [48] A. Schneider, R. Teyssier, J. Stadel, N.E. Chisari, A.M.L. Brun, A. Amara et al., *Quantifying baryon effects on the matter power spectrum and the weak lensing shear correlation*, *Journal of Cosmology and Astroparticle Physics* **2019** (2019) 020–020.
- [49] L. Lucie-Smith, H.V. Peiris, A. Pontzen, A. Halder, J. Schaye, M. Schaller et al., *Cosmological feedback from a halo assembly perspective*, *Physical Review D* **112** (2025) .
- [50] B. Hadzhiyska, S. Ferraro, R. Pakmor, S. Bose, A.M. Delgado, C. Hernández-Aguayo et al., *Interpreting sunyaev-zel'dovich observations with millenniumtng: Mass and environment scaling relations*, 2023.
- [51] Z. Lin, N. Huang, C. Avestruz, W.L.K. Wu, S. Trivedi, J. Caldeira et al., *Deepsz: identification of sunyaev-zel'dovich galaxy clusters using deep learning*, *Monthly Notices of the Royal Astronomical Society* **507** (2021) 4149–4164.
- [52] Z. Zhang, H. Wang, W. Luo, H. Mo, J. Zhang, X. Yang et al., *Halo mass-observable proxy scaling relations and their dependencies on galaxy and group properties*, 2023.
- [53] T.S.O. Collaboration, M. Abitbol, I. Abril-Cabezas, S. Adachi, P. Ade, A.E. Adler et al., *The simons observatory: Science goals and forecasts for the enhanced large aperture telescope*, 2025.
- [54] T. Nishimichi, M. Takada, R. Takahashi, K. Osato, M. Shirasaki, T. Oogi et al., *Dark quest. i. fast and accurate emulation of halo clustering statistics and its application to galaxy clustering*, *The Astrophysical Journal* **884** (2019) 29.
- [55] G. Aricò, R.E. Angulo, S. Contreras, L. Ondaro-Mallea, M. Pellejero-Ibañez and M. Zennaro, *The bacco simulation project: a baryonification emulator with neural networks*, *Monthly Notices of the Royal Astronomical Society* **506** (2021) 4070–4082.